4H-SiC Schottky diode radiation hardness assessment by IBIC microscopy

4H-SiC Schottky diode radiation hardness assessment by IBIC microscopy

[1]Ettore Vittone, [1]Paolo Olivero, [2]Milko Jaksic, [3]Zeljko Pastuovic

[1]Physics Department, University of Torino (I), via P. Giuria 1, 10125 Torino, Italy.

[2]Laboratory for Ion Beam Interactions, Ruđer Bosǩović Institute, Bijenička 54, Zagreb, 10000, Croatia.

[3]Centre for Accelerator Science, Australian Nuclear Science and Technology Organisation, Lucas Heights, 2234, NSW, Australia

Abstract

We report findings on the Ion Beam Induced Charge (IBIC) characterization of a 4H-SiC Schottky barrier diode (SBD), in terms of the modification of the Charge Collection Efficiency (CCE) distribution induced by 20 MeV C ions irradiations with fluences ranging from 20 to 200 ions/μm^2.

The lateral IBIC microscopy with 4 MeV protons over the SBD cross section, carried out on the pristine diode evidenced the widening of the depletion layer extension as function of the applied bias and allowed the measurement of the minority carrier diffusion lengths.

After the irradiation with C ions, lateral IBIC showed a significant modification of the CCE distribution, with a progressive shrinkage of the depletion layer as the fluence of the damaging C ions increases.

A simple electrostatic model ruled out that the shrinkage is due to the implanted charge and ascribed the perturbation of the electrostatic landscape to radiation-induced defects with positive charge state.

Introduction

Silicon carbide (SiC) has highly desirable physical and chemical properties that make it an ideal material for use in a wide variety of applications, ranging from micro-electromechanical systems [1], chemical sensing [2], quantum [3] and electronic devices. In this last field, silicon

carbide, and in particular the 4H-SiC allotrope, plays a key role in power electronics [4] due to its large indirect band gap (~3.2 eV), large breakdown electric field (2 MV cm^{-1}), high electron mobility (900 cm^2 V^{-1} s^{-1}) and high thermal conductivity (400 W m^{-1} K^{-1}) [5]. One of the main elements of interest in this material is represented by the possibility of making SiC-based systems operating at high temperature [6] and, in general, in harsh environments [7], including the development of detectors operating in harsh ionizing radiation conditions [8]. Thanks to its high threshold energy for atomic displacement (24 eV for C and 66 eV for Si [9], to be compared with 21 eV in Si [10] and 50 eV for diamond [11]), SiC is an attractive candidate for the fabrication of radiation detectors [12] for applications ranging from laser-generated plasma diagnostics [13], high energy physics experiments [14], betavoltaics [15], x /gamma ray spectroscopy [16] to neutron monitoring [17] in fission reactors, in high-level radioactive waste [18] and fusion reactors [19], [20].

The assessment of SiC radiation hardness is therefore important for the development of SiC detectors in radiation-intensive environments, and has been the object of several studies, aimed to identify main defects and the relevant recombination levels induced by radiation, which degrade the electronic properties of SiC devices [21] , [22] , [23].

This paper contributes to this subject by reporting the characterization of a 4H-SiC Schottky diode by the Ion Beam Induced Charge technique (IBIC). The advantages of this technique stems from using MeV ions both as damaging and probing agents, which allow both the characterization of the transport and electrostatic properties of semiconductors, as well as the study of damage induced by ion irradiation [24], on the availability of a robust interpretative model [25], and on the possibility of quantitatively mapping the charge collection efficiency (CCE) by using scanning focused ion beams [26].

The experiment here presented and discussed, consists of the IBIC analysis of a 4H-SiC Schottky diode, which was cleaved in order to expose its lateral cross section to 4 MeV proton microbeam to probe the CCE profile (first phase). Subsequently, selected areas of the frontal

Schottky electrode were irradiated with 20 MeV C ion beam with different fluences (second phase). Finally, lateral IBIC analysis was performed in order to investigate the effects of the C ion irradiations on the CCE profiles (third phase).

Experimental

The device under study was a 4H-SiC Schottky diode fabricated on a n-type (~50 μm thick) epitaxial layer on low micropipe density (16–30 cm^{-3}), n^+ substrate from CREE Research Inc.. The Schottky and ohmic electrodes (3 mm in diameter) were deposited by evaporating Ni (100 nm) and Au (100 nm) on the epitaxial layer and a Ti (30 nm) /Pt (30 nm) /Au (150 nm) on the substrate side (C-face), respectively (Fig. 1a,b). An almost constant effective donor concentration of about $1.5 \cdot 10^{14} cm^{-3}$ in the first 30 μm of the n-type region, an ideality factor of (1.14±0.03) and a barrier height of (1.52±0.01) eV were estimated from capacitance and current-voltage characterization.

The diode was cleaved in order to expose its lateral cross section to the ion beam irradiation (lateral IBIC set-up [27]). The cleavage increased the current in the reverse bias conditions due to the leakage current across the cleaved surface. At 100 V the current was maintained below 10 nA, i.e. values still compatible with IBIC measurements (Fig. 1c).

The experiments were carried out at the RBI (Ruđer Bošković Institute) ion microprobe facility. The electronic chain to process the IBIC signal was constituted by a charge sensitive preamplifier (Canberra 2004) and a shaping amplifier (Canberra 2021, shaping time 1.5 μs). The Spector [28] hardware and software system was used for data acquisition and beam scan control. The calibration of the electronic chain was performed by using a reference Si detector to measure signals from 4 MeV protons, resulting in a charge sensitivity of 1800 electrons /channel and a spectral resolution (FWHM) of 1.2×10^4 electrons, which correspond to 14 keV/channel and 94 keV, respectively, in SiC, assuming an average energy to create an electron/hole pair of 7.78 eV [29].

The 4H-SiC SBD diode was irradiated at normal incidence through the surface Schottky contact with 20 MeV carbon ions, with the purpose of creating displacement damage in the active region under reverse biasing. Lateral IBIC measurements to characterise changes in CCE and electric field profile across the depletion region of the SBD were carried out using the probing 4 MeV proton microbeam focused to a spot size of about 2 μm (FWHM), as estimated from of an on-axis scanning transmission ion microscope (STIM) image of a copper grid (2000 mesh pitch). Since the electron/hole generation occurs primarily at the Bragg peak, i.e. at the end of the proton range (about 100 μm from SRIM simulations[30]), surface recombination at the irradiated (cleaved) surface is assumed not to play a dominant role.

Results and Discussion

First phase: IBIC analysis of the pristine diode

The characterization of the 4H-SiC diode by irradiating the cleaved sample from the side (lateral IBIC) was performed using a focused 4 MeV proton beam. The CCE maps (median values) at different bias voltages (V_b) shown in Fig. 2 evidence the presence of a region with high CCE, which widens as V_b increases, followed by a rapid decrease in efficiency, as the distance (y) from the Schottky electrode increases. The CCE profiles, calculated along the y axis of the IBIC maps, corroborate these observations, as shown in Fig. 3.

The interpretation of these profiles can be first approached by the drift-diffusion model, as already adopted in previous IBIC analyses of Si p-n junction and GaAs Schottky diodes [31]: the plateau at 100% efficiency cover the depletion region, where the strong electric field very efficiently drifts both the minority (hole) and majority (electron) charge carriers generated by ionization towards frontal (holes) and back (electrons) electrodes, inducing a charge signal at the sensitive (frontal) electrode, which is processed by the electronic chain.

Fig. 3b shows the good agreement between the extension of the plateaux of the CCE profiles (Fig. 3a) and the extension of the depletion layer extracted from capacitance-voltage characteristic, as function of the applied bias voltage.

The CCE decay at longer distance from the Schottky barrier is to be attributed to the probability of minority carriers, generated in the neutral region, to diffuse to the edge of the depletion region [32]. The logarithmic slope of these CCE decay curves is almost constant for all bias voltage values and is equal to the inverse of the hole diffusion length L_h, which can be estimated as L_h=(4.9±0.3) μm.

More elaborated simulations, based on the IBIC theory derived from the Shockley-Ramo-Gunn theorem, have been carried out by solving the coupled Poisson's, the semiconductor continuity equations and the relevant adjoint equations [33]. These equations have been numerically solved by the finite element method [34], taking as input the doping profile and the Schottky barrier potential value extracted from capacitance–voltage measurements and the hole carrier lifetime (τ_h = 80 ns). The latter value was derived from the diffusion length previously calculated, assuming a diffusivity of 3 cm^2/s [8]. The results of these 1D simulations, shown as continuous lines of Fig. 3a, are in good agreement with the experimental data. An alternative analysis of this device was carried out by P. Olivero et al. [35] by a Monte Carlo method.

Second phase: Frontal electrode irradiation

The irradiation of the frontal electrode was carried out by using 20 MeV C^{4+} focused ion beam, in order to induce radiation damage in selected regions at different fluences ranging from 20 to 200 ions/μm^2. The applied bias voltage during irradiation was 10 V.

Since the ion current was of the order of 10^3 ions/s, the IBIC signals were recorded during the irradiation, both to monitor the IBIC signal degradation and to refine the fluence measurements, which were estimated by the number of detected ions divided by the area of the selected region (namely, 145×68 μm^2). For the highest fluence, we cannot exclude that part of the events fall

below the electronic threshold, so, in this case, the fluence (200 ions/μm^2) can be significantly underestimated.

In this phase of the experiment, it was not possible to calculate the absolute CCE due to the rapid degradation of the reference silicon detector; in the following, the CCE relevant to 20 MeV C ions is calculated by normalizing the IBIC signal to the median of the spectrum in the pristine diode biased at 50 V.

Fig. 4a) shows an example of IBIC spectra taken during the irradiation of region E; the degradation of the median CCE monitored during the irradiation of the 4 regions is shown in Fig. 4b).

After the irradiation, IBIC maps of the sample were taken at different reverse bias voltages (namely, 10 and 50 V) using the same ion beam (20 MeV C), as shown in Fig. 5. The feathered edges of the irradiated regions are due to the limited focus of the C beam, which is of the order of 10 μm.

As expected from previous studies on the radiation hardness of silicon diodes [24], it is apparent that the smaller is the applied bias voltage, the higher is the contrast of the irradiated region in the IBIC map. The depletion layer at a reverse bias voltage of 10 V has a width of ~10 μm (see Fig. 3b). Therefore, a non-negligible fraction of charge carriers is generated by ionization in the neutral region, and in particular at the peak of the vacancy profile (Fig. 6), i.e. in proximity of the highest concentration of damage-induced defects. In this region, the slow diffusion of holes toward the depletion region fosters the recombination, the reduction of the hole lifetime and thus the degradation of the CCE.

At a reverse bias voltage of 50 V, the strong electric field promotes a fast drift of the carriers, which mitigates the recombination effects, resulting in a reduction of contrast in the map in the case of low fluence.

It is worth noticing that these considerations hold also in the case of a significant modification of the diode electrostatics, as shown in the lateral IBIC analysis carried out in the phase 3 of this experiment.

3nd phase: Lateral IBIC of the irradiated regions

In order to gain insight on the origin of the CCE degradation observed during the second phase of the experiment, lateral IBIC analysis of the irradiated regions was carried out, replicating the conditions adopted in the first phase. Fig. 7 shows the CCE maps obtained in lateral IBIC geometry, using 4 MeV protons as the ion probe, at different bias voltages of regions C,D,E,F, that were previously irradiated with 20 MeV C fluences of 20,61,180,200 ions/μm^2, respectively.

The CCE profiles, extracted from the central parts of the irradiated regions, are shown in Fig. 8.

It is apparent that the irradiated regions show a degradation of the CCE profile, which is more evident for higher fluences.

At 10 V bias, i.e. for a depletion layer extension smaller than the 20 MeV C ion range, the profiles show a degradation of the CCE as the ion fluence increases. This behaviour is what expected since the carrier lifetime decreases as the recombination centres induced by radiation increases.

However, it is worth noting that the depth at which full induced charge collection is measured shrinks as the fluence increases, down to a depth (vertical coordinate in Fig. 7) which corresponds to the range of 20 MeV C ions (12.8 µm) in the diode. At the highest fluence (region F), the CCE is higher at this depth, where the vacancy peak, and then the highest recombination, occurs.

Looking specifically at the regions C and D (fluence 20 and 61 ions/μm^2, respectively) for V_b=50 and 100 V, the CCE exponential decay occurs at a depth which is larger than the C ion range (R). There, the lifetime values (and thus diffusion length values) of the minority carriers

are not affected by damage effects and the logarithmic slopes of the CCE profiles in these two regions at the highest bias voltages are almost identical.

It is apparent that the shrinkage of the depletion region is the dominant effect of the 20 MeV C ion irradiation, and it can be ascribed to a modification of the diode electrostatics landscape. Actually, this evidence can be interpreted by a simple electrostatic model, which assumes that the modification of the effective charge density is induced by the damage proportional to the ion fluence confined in a planar interface located at peak of the damage production (Fig. 6). This assumption can be considered a good approximation to the real damage profile, since the longitudinal straggling of the damage profile is small in comparison to the projected range [30]. Assuming a surface charge located at the C ion range (R=12.8 μm) emerging from a flat donor distribution (N_D=1.5·$10^{14}$$cm^{-3}$), the shrinkage can be related to the ion fluence through the expression

1) $(w_0^2 - w^2) = \frac{2R}{N_D}\alpha\varphi$

where α it the ratio of the surface density of positive charge generated by ion damage and the C ion fluence (φ). The derivation of eq. 1) is given in the appendix. The linear fit shown in Fig. 9 provides a value of α of about 70, a value which rules out the hypothesis that the shrinkage of the depletion region is merely due to the implanted charge. Therefore, these positive charges could consist of radiation-induced electrically active defects, whose density is related to the number of defects generated by single 20 MeV C (Fig. 6), given the number of displaced atoms per ion (about 200 Si and 400 C), as computed by SRIM simulation [30]. Since such defects increase the space charge in the depletion region, we infer their positive charge state.

The change in effective doping in the space-charge region induced by radiation induced defects is a well-known effect in semiconductor detectors [36] and direct evidence of local effects of electrically active defects on the internal electric field has been observed in diamond [37]. However, our interpretation is in apparent disagreement with previous studies, which ascribe the irradiation effects in Schottky [22] and p-n [23] 4H-SiC diodes, irradiated with 7

MeV C and 700 keV He and ions, respectively, to doping compensation. However, the studies of Izzo et al. [22] and Pellegrino et al. [23] are based on the analysis of the current-voltage characteristics in forward steady-state conditions, and the apparent increase of the series resistance is associated to a decrease in the concentration of free carriers in the neutral region. It is worth remarking that the IBIC analysis described in this paper was performed in reverse polarization condition and the shrinking of the region where CCE=100%, i.e. the region where carriers induce charge at the sensing electrode, suggests a modification of the electrostatics, which does not necessarily coincide with a modification of the free carrier concentration.

Our model can be extended to interpret all the other profiles shown in Fig. 8. At V_b=20 V, the logarithmic slope of the profile in region C is apparently steeper than that the one which is relevant to the pristine region. Taking into account that this exponential decay occurs in the neutral region, where diffusion mechanism inject the minority carriers in the depletion region, the more rapid decay of the CCE profile can be ascribed to the increase of the recombination centers generated at the end of the ion range, which decreases the minority carrier lifetime and diffusion length. As the C ion fluence increases (regions D, E, F), the progressive decrease of lifetime value degrades the drift length of both the carriers and then the IBIC signal, as induced by the drift of charge carriers in the depletion regions. Similar consideration can be applied also for V_b=50 V and V_b=100 V. In particular, it is worth noting that in region E, the CCE profile is peaked at the depth corresponding to the C ion range, where the recombination should be maximum. These counter-intuitive results can be explained by assuming that, consistently with our model, at this depth a significant increase of the electric field occurs, which compensates the reduction of drift length due to the degradation of the carrier lifetime.

Conclusions

In this work, IBIC analysis of a 4H-SiC Schottky diodes was performed in order to investigate the performances of this device in view of its application as ionizing particle detector. The

experiments were conducted in lateral geometry, i.e. by raster scanning the 4 MeV proton microbeam over the cleaved cross section of the diode.

The CCE maps of the pristine diode show regions of maximum efficiency which widens as the reverse applied bias increases, in agreement with the results emerging from the standard electronic characterization; the analysis of the CCE exponential decay in the neutral region allowed the calculation of the minority carrier diffusion length.

In order to evaluate the effects of high energy ion irradiation on the device performances, selected areas of the diode were exposed to 20 MeV C ion beam at different fluences.

The following lateral IBIC experiments showed a significant modification of the CCE distribution which could not be interpreted by ascribing the CCE degradation only to the increase of recombination centres induced by the radiation. Actually, the most evident effect at low fluence and high bias voltage was represented by the shrinkage of the depletion layer width, which suggests a modification of the diode electrostatics landscape induced by defects generated by the 20 MeV C ion irradiation. A simple model was introduced, which describes the electrostatic effects assuming a planar interface placed at the depth of maximum damage with a charge surface density proportional to the ion fluence. The results of this analysis indicate that this shrinkage is due to the charge implanted by the C ions and can reasonably be ascribed to the creation of defects assuming positive charge states in the space charge region. Such an interpretation is further corroborated by the presence of a peak of CCE located at the 20 MeV C ion range: the increase of the electric field in the space charge region compensates the reduction of the carrier lifetime, which was expected to degrade the carrier mean drift length and then the induced charge signal.

These results evidence radiation induced effects not considered in previous studies, and can trigger further analyses to assess the radiation hardness of 4H-SiC devices.

Acknowledgement

This work was supported by the project 'Departments of Excellence' (L. 232/2016), funded by the Italian Ministry of Education, University and Research (MIUR). We would like to acknowledge the Australian Government funding for ANSTO Centre for Accelerator Science through the National Collaborative Research Infrastructure Strategy (NCRIS) project.

Appendix: derivation of eq. 1)

In a 1-dimensional model, the relationship between the space charge distribution ρ and the electric field $\mathcal{E}$ is given by the Gauss equation [38]:

A.1) $$\frac{d\mathcal{E}}{dx} = +\frac{\rho}{\epsilon}$$

Where ϵ is the silicon dielectric constant.

In the full depletion approximation, i.e. assuming a region completely depleted of mobile carriers, the space charge distribution is proportional to the density of effective donors D, which is assumed to be the sum of a constant doping profile (N_D) and a Dirac-delta like distribution of donors generated by radiation and centred at R (range of the damaging ion in silicon):

A.2) $$\rho(x) = q \cdot D(x) = q \cdot N_D + q \cdot S \cdot \delta(x - R) = q \cdot N_D + q \cdot \alpha \cdot \varphi \cdot \delta(x - R)$$

Where q is the elementary charge, S is the surface density of radiation induced donors, which is assumed proportional to the damaging ion fluence:

A.3) $$S = \alpha \cdot \varphi$$

The dominion of eq. A.1) is in the range [0,w], where w is the extension of the depletion region.

The solution of eq. A.1) is

A.4) $$\mathcal{E}(x) = +\frac{qN_D}{\epsilon}(x - w) - \frac{q\alpha\varphi}{\epsilon}\theta(R - x)$$

Where θ is the Heaviside's step function and this expression fulfil the boundary condition $\mathcal{E}(x = w) = 0$

The electrostatic potential ψ can then be calculated by integrating the electric field, i.e.

A.5) $$\psi(x) = -\int_0^x \mathcal{E}(x)dx =$$

$$= (-V_{bi} - V_b) - \frac{qN_D}{2\epsilon}x^2 + x\left(\frac{qN_D}{\epsilon}w + \frac{q\alpha\varphi}{\epsilon}\right) - \frac{q\alpha\varphi}{\epsilon}(x-R)\,\theta(x-R)$$

Which fulfils the boundary condition:

A.6) $\psi(x=0) = (-V_{bi} - V_b)$

Where V_{bi} is the built in potential and V_b is the applied bias voltage at the Schottky electrode.

The condition at the boundary of the depletion region:

A.7) $\psi(x=w) = 0$

leads to the following:

A.8) $(-V_{bi} - V_b) + \frac{qN_D}{2\epsilon}w^2 + \frac{q\alpha\varphi}{\epsilon}w - \frac{q\alpha\varphi}{\epsilon}(w-R) = 0 \Rightarrow$

$$\Rightarrow w^2 = \frac{2\epsilon(V_{bi}+V_b)}{qN_D} - \frac{2R\alpha}{N_D}\varphi \Rightarrow w_0^2 - w^2 = \frac{2\cdot\alpha\cdot R}{N_D}\varphi$$

Where $w_0 = \sqrt{\frac{2\varepsilon(V_b+V_{bi})}{q\cdot N_D}}$ is the extension of the depletion region of the pristine diode (i.e. when $\varphi = 0$).

Just as an example, Fig. A. 1a,b show the profiles of the electrostatic potential and of the electric field, respectively, calculated for V_b=100 V and for different fluences, assuming the value of $\alpha = 70$ extracted from the linear fit of Fig. 9. From these graphs, it is apparent the shrinkage of the depletion region (eq. A.8) and the increase of the electric field for x<R.

Fig. A. 1c,d show the weighting Gunn's potential and the Gunn's weighting field calculated through the derivative of of the electrostatic potential (eq. A.5) and of the electric field (eq. A.5) with respect to the applied bias voltage V_b , i.e. $\frac{\partial\psi}{\partial V_b}$ and $\frac{\partial\varepsilon}{\partial V_b}$, respectively [39]. As expected, they turn out to be respectively $\frac{\partial\psi}{\partial V_b} = \left(-1+\frac{x}{w}\right)\cdot\vartheta(w-x)$ and $\frac{\partial\varepsilon}{\partial V_b} = -\frac{\vartheta(w-x)}{w}$ and furtherly demonstrate that the active region of the diode, i.e. the region where the drift of the carrier induce the charge at the sensitive electrode, shrinks because of the space charge generated by irradiation.

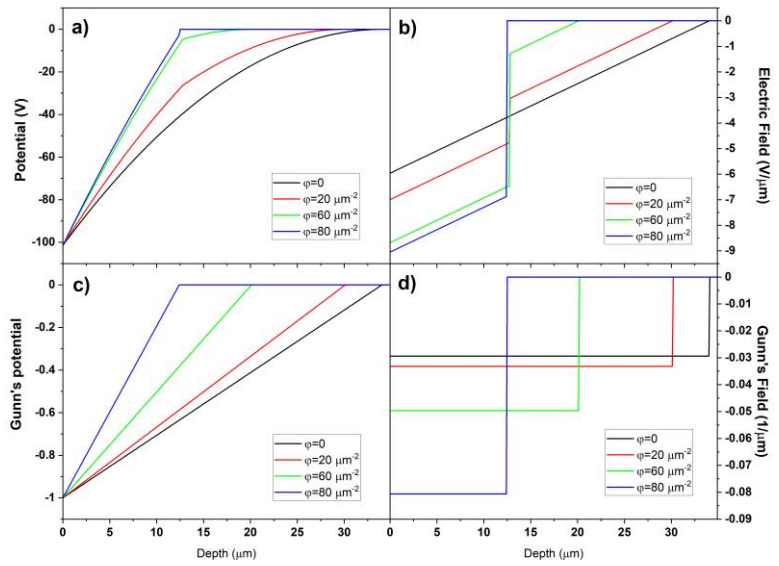

Fig. A. 1: a) electrostatic potential (eq. A.5) , b) electric field (eq. A.4) , c) Gunn's weighting potential, d) Gunn's weighting field profiles calculated from the model described in the appendix, using the following parameters: R=12.8 μm, α=70, N_D=1.5·10^8 μm^{-3}, V_{bi}=1.5 V, V_b=100 V.

List of references

[1] B. S. Sviličić, E. Mastropaolo, B. Flynn, and R. Cheung, "Electrothermally Actuated and Piezoelectrically Sensed Silicon Carbide Tunable MEMS Resonator," *IEEE ELECTRON DEVICE Lett.*, vol. 33, no. 2, 2012, doi: 10.1109/LED.2011.2177513.

[2] A. R. Kermany, J. S. Bennett, V. M. Valenzuela, W. P. Bowen, and F. Iacopi, "Potential of epitaxial silicon carbide microbeam resonators for chemical sensing," *Physica Status Solidi (A) Applications and Materials Science*, vol. 214, no. 4. Wiley-VCH Verlag, Apr.

01, 2017, doi: 10.1002/pssa.201600437.

[3] G. Pacchioni, “A high-fidelity interface between spins and photons,” *Nat. Publ. Gr.*, vol. 2, 2017, doi: 10.1038/natrevmats.2017.52.

[4] Eddy C. R. Jr. and Gaski D. K., “Silicon Carbide as a Platform for Power Electronics,” *Science (80-.).*, pp. 1398–1400, 2009, doi: 10.1126/science.1175869.

[5] A. Elasser and T. P. Chow, “Silicon carbide benefits and advantages for power electronics circuits and systems,” *Proceedings of the IEEE*, vol. 90, no. 6. Institute of Electrical and Electronics Engineers Inc., pp. 969–986, 2002, doi: 10.1109/JPROC.2002.1021562.

[6] C. Buttay *et al.*, “State of the art of high temperature power electronics,” *Mater. Sci. Eng. B Solid-State Mater. Adv. Technol.*, vol. 176, no. 4, pp. 283–288, 2011, doi: 10.1016/j.mseb.2010.10.003.

[7] A. Hassan, Y. Savaria, and M. Sawan, “Electronics and packaging intended for emerging harsh environment applications: A review,” *IEEE Trans. Very Large Scale Integr. Syst.*, vol. 26, no. 10, pp. 2085–2098, 2018, doi: 10.1109/TVLSI.2018.2834499.

[8] F. Nava, G. Bertuccio, A. Cavallini, and E. Vittone, “Silicon carbide and its use as a radiation detector material,” *Meas. Sci. Technol.*, vol. 19, no. 10, 2008, doi: 10.1088/0957-0233/19/10/102001.

[9] W. Li *et al.*, “Threshold displacement energies and displacement cascades in 4H-SiC: Molecular dynamic simulations,” *AIP Adv.*, vol. 9, no. 5, pp. 8–13, 2019, doi: 10.1063/1.5093576.

[10] S. R. Messenger, E. A. Burke, M. A. Xapsos, G. P. Summers, and R. J. Walters, “The simulation of damage tracks in silicon,” *Eur. Sp. Agency, (Special Publ. ESA SP*, vol. 2003-Septe, no. 5, pp. 363–367, 2003.

[11] S. Ditalia Tchernij *et al.*, “Electrical characterization of a graphite-diamond-graphite junction fabricated by MeV carbon implantation,” *Diam. Relat. Mater.*, vol. 74, pp. 125–

131, 2017, doi: 10.1016/j.diamond.2017.02.019.

[12] J. M. Rafi *et al.*, “Electron, Neutron, and Proton Irradiation Effects on SiC Radiation Detectors,” *IEEE Trans. Nucl. Sci.*, vol. 67, no. 12, pp. 2481–2489, 2020, doi: 10.1109/TNS.2020.3029730.

[13] G. Bertuccio, D. Puglisi, L. Torrisi, and C. Lanzieri, “Silicon carbide detector for laser-generated plasma radiation,” *Appl. Surf. Sci.*, vol. 272, pp. 128–131, 2013, doi: 10.1016/j.apsusc.2012.03.183.

[14] T. Kishishita *et al.*, “SiC P+N junction diodes toward beam monitor applications,” *IEEE Trans. Nucl. Sci.*, vol. 68, no. 12, pp. 2787–2793, 2021, doi: 10.1109/TNS.2021.3118788.

[15] J. Russo *et al.*, “Planar and textured surface optimization for a tritium-based betavoltaic nuclear,” *Int J Energy Res.*, vol. 43, pp. 4370–4389, 2019.

[16] O. F. Karadavut, S. K. Chaudhuri, J. W. Kleppinger, R. Nag, and K. C. Mandal, “Performance-improved vertical Ni/SiO2/4H-SiC metal-oxide-semiconductor capacitors for high-resolution radiation detection,” *IEEE Trans. Nucl. Sci.*, vol. 69, no. 8, pp. 1965–1971, 2022, doi: 10.1109/TNS.2022.3168792.

[17] A. Lo Giudice *et al.*, “Performances of 4H-SiC Schottky diodes as neutron detectors,” *Nucl. Instruments Methods Phys. Res. Sect. A Accel. Spectrometers, Detect. Assoc. Equip.*, vol. 583, no. 1, 2007, doi: 10.1016/j.nima.2007.08.241.

[18] F. H. Ruddy, L. Ottaviani, A. Lyoussi, C. Destouches, O. Palais, and C. Reynard-Carette, “Silicon Carbide Neutron Detectors for Harsh Nuclear Environments: A Review of the State of the Art,” *IEEE Trans. Nucl. Sci.*, vol. 69, no. 4, pp. 792–803, 2022, doi: 10.1109/TNS.2022.3144125.

[19] B. Hong *et al.*, “Diagnostic of Fusion Neutrons on EAST Tokamak Using 4H-SiC Detector,” *IEEE Trans. Nucl. Sci.*, vol. 69, no. 3, pp. 639–644, 2022, doi: 10.1109/TNS.2022.3146180.

[20] L. Liu, A. Liu, S. Bai, L. Lv, P. Jin, and X. Ouyang, “Radiation resistance of silicon carbide schottky diode detectors in D-T fusion neutron detection,” *Sci. Rep.*, vol. 7, no. 1, pp. 1–8, 2017, doi: 10.1038/s41598-017-13715-3.

[21] I. Capan, “4H-SiC Schottky Barrier Diodes as Radiation Detectors: A Review,” *Electron.*, vol. 11, no. 4, 2022, doi: 10.3390/electronics11040532.

[22] Izzo G., Litrico G., Calcagno L., Foti G., and La via F., “Electrical properties of high energy ion irradiated Schottky diodes,” *J. Appl. Phys.*, vol. 104, no. 9, 2008, doi: 10.1063/1.3018456.

[23] D. Pellegrino, L. Calcagno, M. Zimbone, S. Di Franco, and A. Sciuto, “materials Correlation between Defects and Electrical Performances of Ion-Irradiated 4H-SiC p-n Junctions,” *Materials (Basel).*, vol. 14, 2021, doi: 10.3390/ma14081966.

[24] E. Vittone *et al.*, “Charge collection efficiency degradation induced by MeV ions in semiconductor devices : Model and experiment,” *Nucl. Inst. Methods Phys. Res. B*, vol. 372, pp. 128–142, 2016, doi: 10.1016/j.nimb.2016.01.030.

[25] E. Vittone, “Theory of ion beam induced charge measurement in semiconductor devices based on the Gunn’s theorem,” *Nucl. Instruments Methods Phys. Res. Sect. B Beam Interact. with Mater. Atoms*, vol. 219–220, no. 1–4, pp. 1043–1050, 2004, doi: 10.1016/j.nimb.2004.01.210.

[26] E. Vittone *et al.*, “Semiconductor characterization by scanning ion beam induced charge (IBIC) microscopy,” *Nucl. Instruments Methods Phys. Res. Sect. B Beam Interact. with Mater. Atoms*, vol. 266, no. 8, 2008, doi: 10.1016/j.nimb.2007.12.083.

[27] A. Lo Giudice *et al.*, “Lateral IBIC characterization of single crystal synthetic diamond detectors,” *Phys. Status Solidi - Rapid Res. Lett.*, vol. 5, no. 2, pp. 80–82, 2011, doi: 10.1002/pssr.201004488.

[28] M. Jakšić *et al.*, “New capabilities of the Zagreb ion microbeam system,” *Nucl. Instruments Methods Phys. Res. Sect. B Beam Interact. with Mater. Atoms*, vol. 260, no.

1, pp. 114–118, 2007, doi: 10.1016/j.nimb.2007.01.252.

[29] A. Lo Giudice, F. Fizzotti, C. Manfredotti, E. Vittone, and F. Nava, "Average energy dissipated by mega-electron-volt hydrogen and helium ions per electron-hole pair generation in 4H-SiC," *Appl. Phys. Lett.*, vol. 87, no. 22, p. 222105, 2005, doi: 10.1063/1.2135507.

[30] J. F. Ziegler, M. D. Ziegler, and J. P. Biersack, "SRIM - The stopping and range of ions in matter (2010)," *Nucl. Instruments Methods Phys. Res. Sect. B Beam Interact. with Mater. Atoms*, vol. 268, no. 11–12, pp. 1818–1823, 2010, doi: 10.1016/j.nimb.2010.02.091.

[31] M. B. H. Breese, E. Vittone, G. Vizkelethy, and P. J. Sellin, "A review of ion beam induced charge microscopy," *Nucl. Instruments Methods Phys. Res. Sect. B Beam Interact. with Mater. Atoms*, vol. 264, no. 2, pp. 345–360, Nov. 2007, doi: 10.1016/J.NIMB.2007.09.031.

[32] M. B. H. Breese, "A theory of ion beam induced charge collection," *J. Appl. Phys.*, vol. 74, no. 6, pp. 3789–3799, 1993.

[33] N. Barbero *et al.*, "Degradation of the charge collection efficiency of an n-type Fz silicon diode subjected to MeV proton irradiation," *Nucl. Instruments Methods Phys. Res. Sect. B Beam Interact. with Mater. Atoms*, vol. 348, pp. 260–264, 2015, doi: 10.1016/j.nimb.2014.11.019.

[34] "COMSOL, Multiphysics Modelling and Simulation." [Online]. Available: www.comsol.com.

[35] P. Olivero *et al.*, "Monte Carlo analysis of a lateral IBIC experiment on a 4H-SiC Schottky diode," *Nucl. Instruments Methods Phys. Res. Sect. B Beam Interact. with Mater. Atoms*, vol. 269, no. 20, pp. 2350–2354, 2011, doi: 10.1016/j.nimb.2011.02.020.

[36] G. Lutz, *Semiconductor Radiation Detectors*, 2nd ed. Springer-Verlag, 1999.

[37] J. Forneris *et al.*, "Mapping the Local Spatial Charge in Defective Diamond by Means

of N- V Sensors - A Self-Diagnostic Concept," *Phys. Rev. Appl.*, vol. 10, no. 1, pp. 1–15, 2018, doi: 10.1103/PhysRevApplied.10.014024.

[38] S. M. Sze and K. K. Ng, *Physics of Semiconductor Devices*. 2007.

[39] E. Vittone *et al.*, "Charge collection efficiency degradation induced by MeV ions in semiconductor devices: Model and experiment," *Nucl. Instruments Methods Phys. Res. Sect. B Beam Interact. with Mater. Atoms*, vol. 372, pp. 128–142, 2016, doi: 10.1016/j.nimb.2016.01.030.

Figures

a) 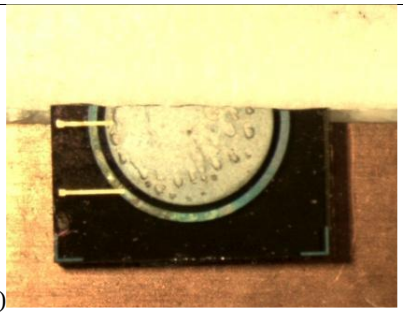

b) 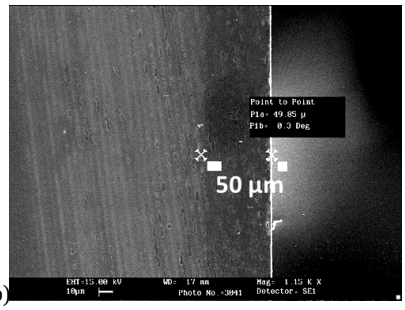

c) 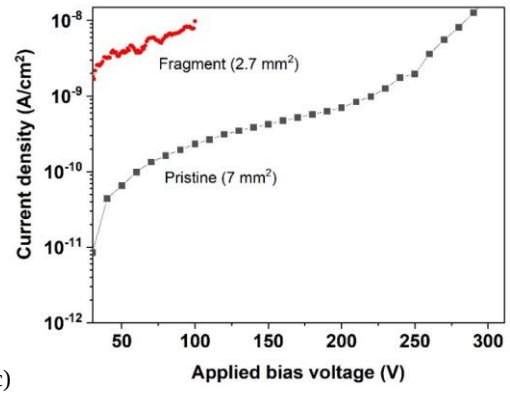

Fig. 1:a) photograph of the cleaved sample; b) SEM image of the cross section; c) current/voltage characteristics before and after the cleavage

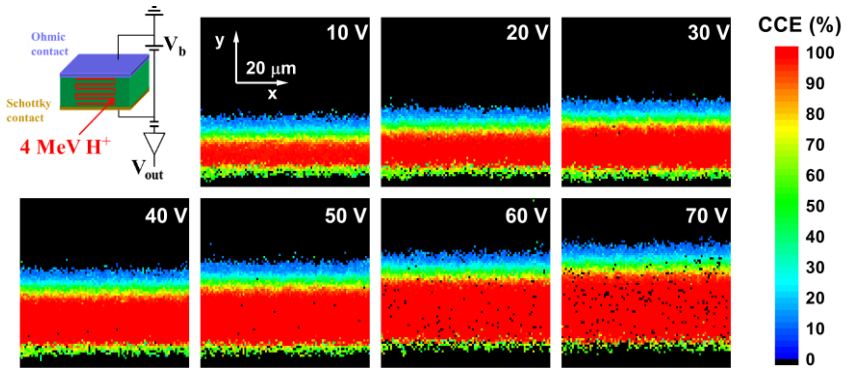

Fig. 2: : Scheme of the lateral IBIC set-up (top left) and CCE distributions resulting from lateral IBIC experiment at different applied bias voltages (V_b). The Schottky electrode is at the bottom of the coloured maps.

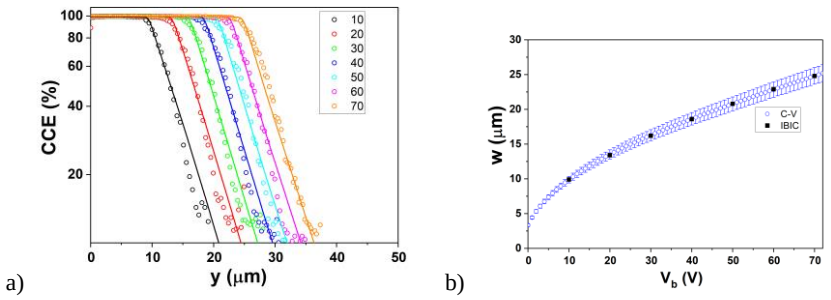

Fig. 3: a) CCE experimental (markers) profiles at different bias voltages (Vb) extracted from the CCE distributions shown in Fig. 2. Lines are the simulated profiles. b) extension of the depletion region (w) as function of the applied bias voltage as extracted from capacitance-voltage characteristics (open circles) and from the extension of the plateaux of the CCE profiles (filled squares calculated from the peak of the derivatives of the simulated curves in a). The error bar is mainly due to the uncertainty (about 10%) of the effective electrode area.

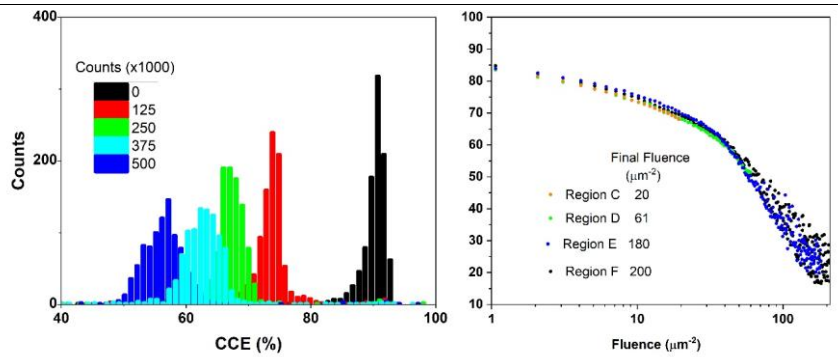

Fig. 4: a) IBIC spectra (1000 counts) taken during the irradiation of the region E at different fluences; V_b=10 V. b) evolution of the median CCE as function of the fluence of the six different irradiated regions. The CCE values are referred to the maximum CCE obtained at 50 V for the pristine sample.

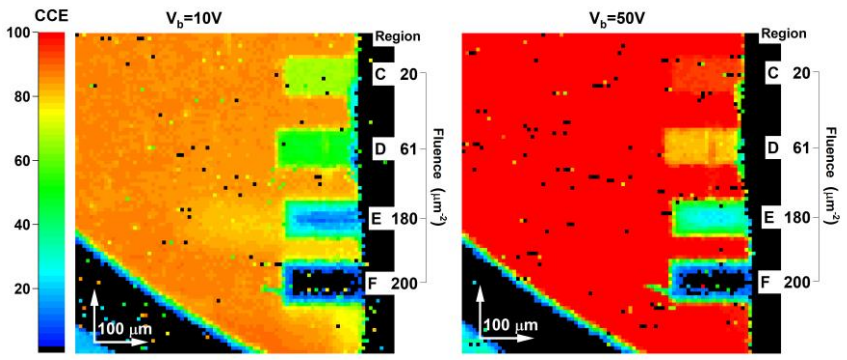

Fig. 5: Frontal IBIC distributions using 20 MeV C ions taken with a bias voltage of 10 V and 50 after irradiation of 4 selected areas at different fluences. The CCE values are referred to the maximum CCE obtained at 50 V for the pristine sample.

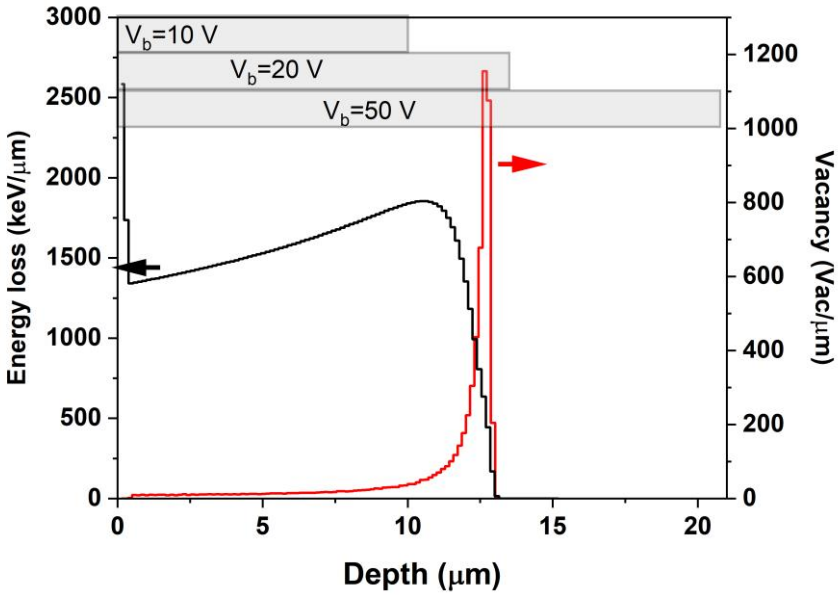

Fig. 6: Energy loss profile (left scale) and vacancy profile (right scale) of 20 MeV C ions in SiC, from SRIM simulation [30]. The grey rectangles indicate the extension of the depletion region @ 10, 20 and 50 V bias voltage.

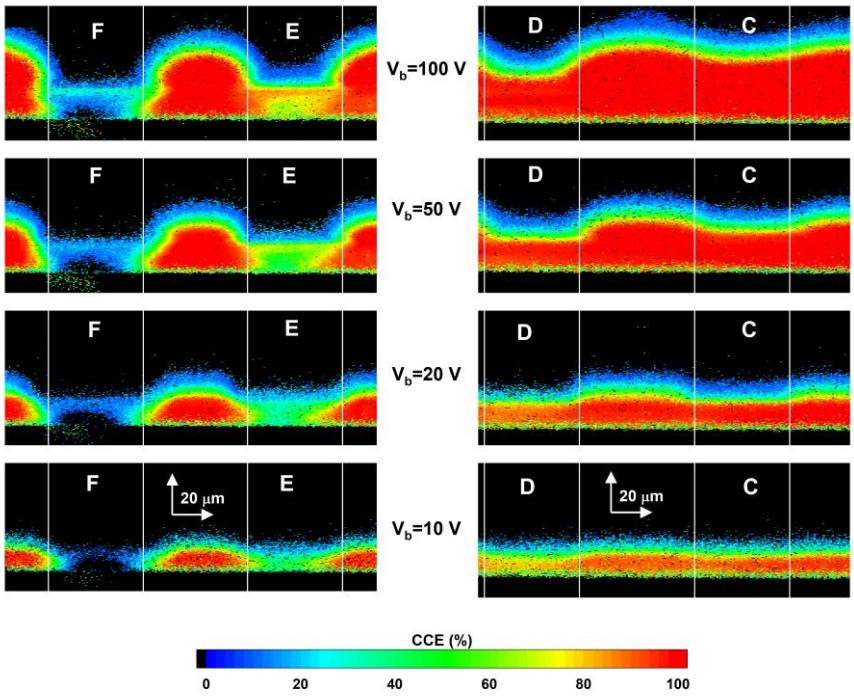

Fig. 7: CCE distributions of the cross section of the irradiated regions C,D,E,F (see Fig. 5) at different bias voltages. The Schottky electrode is at the bottom of the coloured maps.

Eliminato: Fig. 5

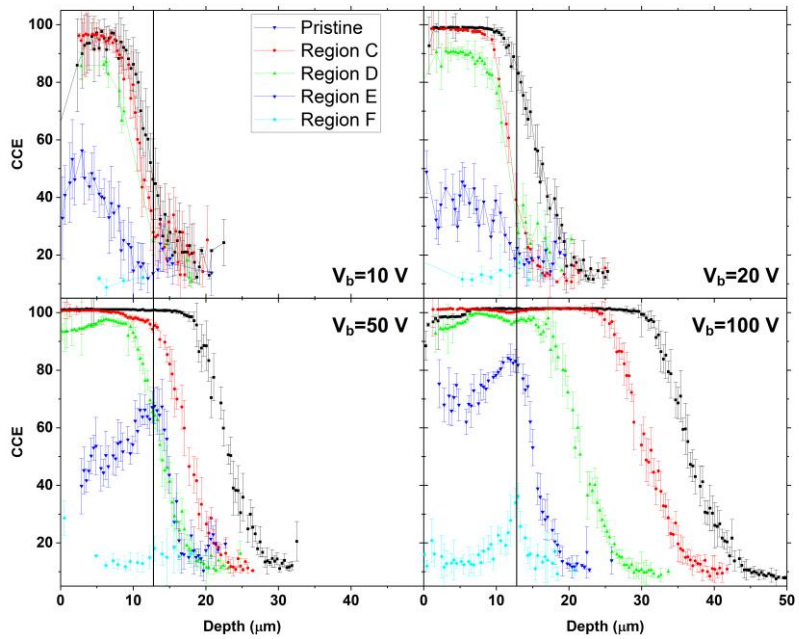

Fig. 8: CCE profiles extracted from the central part of the damaged regions shown in Fig. 7 for bias voltages V_b=10, 20, 50, 100 V. The vertical line at 12.8 μm indicates the position of the peak of the vacancy profile generated by 20 MeV C ions (see Fig. 6).

Eliminato: Fig. 7

Eliminato: Fig. 6

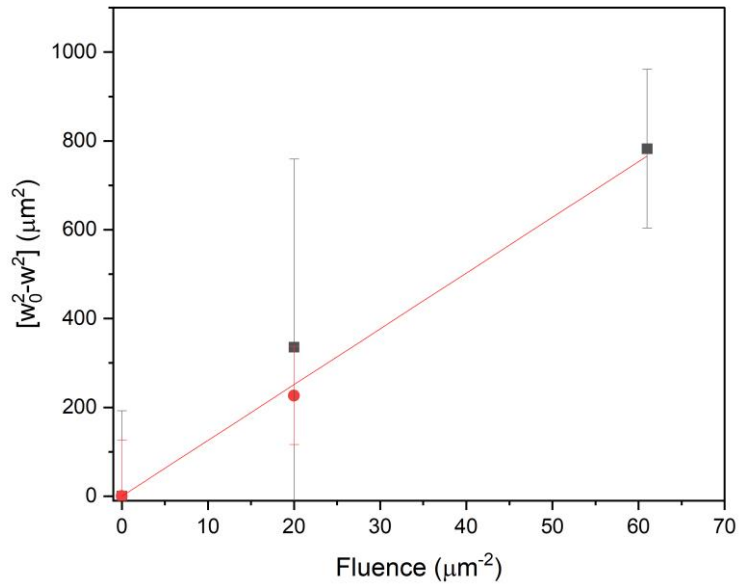

Fig. 9: difference in quadrature of the depletion layer of the C and D irradiated regions and the pristine region vs. the ion fluence. Black markers indicate values extracted from the CCE maps at V_b=100 V; red markers at V_b=50 V. The red line is the linear fit.